Highly efficient desalination performance of carbon honeycomb based reverse osmosis membranes unveiled by molecular dynamics simulations

Qin Qin, Xingyan Liu, Hanxiao Wang, Ting Wei Sun, Fuqiang Chu, Lu Xie, Pascal Brault, Qing Peng

Highly efficient desalination performance of carbon honeycomb based reverse osmosis membranes unveiled by molecular dynamics simulations

To cite this article before publication: Qin Qin *et al* 2021 *Nanotechnology* in press https://doi.org/10.1088/1361-6528/ac03d8

Highly efficient desalination performance of carbon honeycomb based reverse osmosis membranes unveiled by molecular dynamics simulations

Qin Qin[1], Xingyan Liu[1], Hanxiao Wang[2], Tingwei sun[1], Fuqiang Chu[3], Lu Xie[1,*], Pascal Brault[4,*], and Qing Peng[5,6*]

[1]*School of Mechanical Engineering, University of Science and Technology Beijing, Beijing 100083, PR China.*

[2]*China Nuclear Power Technology Research Institute Co., Ltd., Reactor Engineering and Safety Research Center, Shenzhen 518031, China*

[3]*School of Energy and Environmental Engineering, University of Science and Technology Beijing, Beijing 100083, PR China.*

[4]*GREMI UMR7344 CNRS, Université d'Orléans, BP6744, 45067 Orleans Cedex 2, France.*

[5]*Physics Department, King Fahd University of Petroleum & Minerals, Dhahran 31261, Saudi Arabia*

[6]*K.A.CARE Energy Research & Innovation Center at Dhahran, Dhahran, 31261, Saudi Arabia*

* Corresponding emails: xielu@ustb.edu.cn (L. X.), pascal.brault@univ-orleans.fr (P. B.) and qing.peng@kfupm.edu.sa (Q. P.)

Abstract

Seawater desalination is vital to our modern civilization. Here, we report that the carbon honeycomb (CHC) has an outstanding water permeability and salt rejection in the seawater desalination, as revealed by molecular dynamics simulations. More than 92% of ions are rejected by CHC at applied pressures ranging from 50 to 250 MPa. CHC has a perfect salt rejection at pressures below 150Mpa.On increasing the applied pressure up to 150 MPa, the salt rejection reduces only to 92%. Pressure, temperature and temperature gradient are noted to play a significant role in modulating the water flux. The water flux increases with pressure and temperature. With the introduction of a temperature gradient of 3.5 K/nm, the seawater permeability increases by 33% as compared to room temperature. The water permeability of the carbon honeycomb is greater than other carbon materials and osmosis membranes including graphene (8.7 times) and graphyne (2.1 times). It indicates the significant potential of the carbon honeycomb for commercial application in water purification.

Keywords: Carbon honeycomb; Desalination; Molecular dynamics simulation; Temperature gradient

1. Introduction

The production of fresh water is a significant challenge for the increasing population in the society [1]. Seawater desalination is vital to sustain the modern civilization of human beings as one of the most important sources for obtaining fresh water from the oceans and brackish reservoirs [2]. The reverse osmosis technology, which uses the pressure difference as a driving force to filter impurities, accounts for nearly half of the extent of water obtained from desalination [3], where the osmosis membranes play a crucial part, however, still suffer from instability and low efficiency.

The reverse osmosis membranes play an essential role in osmosis desalination and need to exhibit optimal stability, high water permeability and salt rejection for large-scale applications. Currently, commercial reverse osmosis membranes are widely used for salt rejection, however, the low water permeability (about 1 L/(m^2·h·Bar)) and high capital costs have limited the development of such commercial membranes for water treatment [4]. Moreover, the conventional reverse osmosis membranes degrade in the presence of chlorine and are easily fouled by the organic matter [5]. In this respect, many research efforts have been made to develop new nanoporous membrane materials with much higher stability and effective water desalination performance.

Carbon is known to be a flexible element with high stability. It can take form of various allotropes, such as carbon nanotubes (CNT), graphene and graphyne, with a varying arrangement of atoms. Recently, CNT [6-8], graphyne [9] and graphene [10, 11] have been extensively studied for water desalination using both experiments and simulations. In particular, the experimental studies have shown that the porous CNT membranes have a water permeability and salt rejection much higher than the currently used commercial membranes [6], and the water flux increases with decreasing the membrane thickness [8]. Similarly, graphyne membranes have been widely investigated

as porous carbon nanomaterial for desalination, and the results show that water can permeate swiftly through graphyne with high salt rejection [9]. Recently, nanopores have been introduced into graphene's structure. Graphene can also be introduced into a variety of chemically functionalized nanopores (for example, MoS_2 functionalized, hydroxylated and hydrogenated pores) and has been demonstrated to exhibit several orders of magnitude higher water permeability [10-13]. With high water permeability and salt rejection, porous carbon nanomaterials have a high potential of commercial applications.

Pressure gradient is commonly used to generate controlled water flow in the nanoscale desalination membranes [2]. In addition, the introduction of temperature gradient has been proved to induce water flow in the nanoscale porous nanomaterials. Harvey et al. [14] studied the translation motion of the water nanodroplets driven by the temperature gradient in CNT. It was reported that the water flow imposed by the temperature gradient could be controlled [15]. The thermo-diffusion caused by the temperature gradient is known as the Soret effect or thermophoresis [16, 17].

Carbon honeycomb (CHC), a new kind of nanoporous carbon nanomaterials, has been proposed by Park et al.[18]. The special honeycomb-like structure of CHC has attracted a significant research attention since then. The sp^2-sp^3 hybridized CHC was reported to have an outstanding stability with relatively small density and high specific surface per unit volume [19]. Krainyukova et al. [20] experimentally developed stable CHC for the first time. Since then, the structure and properties of CHC have been widely explored [21]. CHC has excellent performance in liquid storage [20], along with enhancement of thermal conductivity [22], electrical conductivity [23] and mechanical properties [24-26]. For example, it was reported that the thermal conductivity of CHC in the cell axis direction was up to 100 W/mK with a density as low as 0.4 g/cm^3, and the specific strength was higher than the other carbon materials [24].

The aforementioned unique properties might be attributed to the distinctive structure: CHC essentially constitutes the rows of honeycomb holes. Rationally, it motivates the research community to further explore its properties and applications in desalination. Herein, a CHC with sp^2 bonding in the wall and sp^3 bonding in the junction has been constructed, and the water desalination performance as a function of applied hydrostatic pressure and length have been investigated using the non-equilibrium molecular dynamics (NEMD) simulations. The effect of temperature and temperature gradient has also been investigated.

2. Models and Methods

Tilted view of CHC is shown in Figure 1(a). As a kind of asymmetrical armchair sp^2–sp^3 bonded carbon honeycomb [27], it consists of graphene nanoribbons. The cross-section is a honeycomb-like structure based on a regular hexagon with side length of 5.8 Å. Each CHC unit consists of four pores (Figure 1(b)) with periodic boundary conditions in both x and y directions. The junction consists of an 8-carbon and two 5-carbon atom rings (as shown in Figure 1(c)).

The water desalination system is composed of two graphene sheets as rigid piston at the two ends of the simulation system along the z-axis, a CHC, salt water in the feed side and fresh water in the permeate side (Figure 1 (d)). According to Robert S. Weatherup [28], water will not escape from graphene and penetrate into the vacuum. The saltwater in the feed side consists of 12 Na ions, 12 Cl ions and 1200 water molecules (20×17×104 Å.). This, thus, produces a salt water area with salinity of 32 $g \cdot L^{-1}$, which is close to the salinity of seawater. Fresh water contains 300 water molecules with a size of 20×17×26 Å. Besides, period boundary conditions are used in all directions, along with two 35 Å vacuum layers placed at the two ends of the graphene piston so that no interaction occurs

between the left and right pistons. Therefore, with the length of CHC as 5.8 nm, the size of the simulation box is about 20×17×258 Å. As the size of the simulation box becomes larger, it has a little effect on the obtained results. We studied the water flux by periodically replicating both x and y directions three times at 50 MPa. This way, the simulation box was enlarged by nine times. The difference in the water flux between the enlarged structure and pristine one is within 5%, implying that the result with such a simulation box is converged and independent of system size. In order to express the system structure more clearly, the simulation system with only 5.8 nm CHC has been shown in Figure 1d. The different lengths of CHC are shown in Supplementary Figure S1.

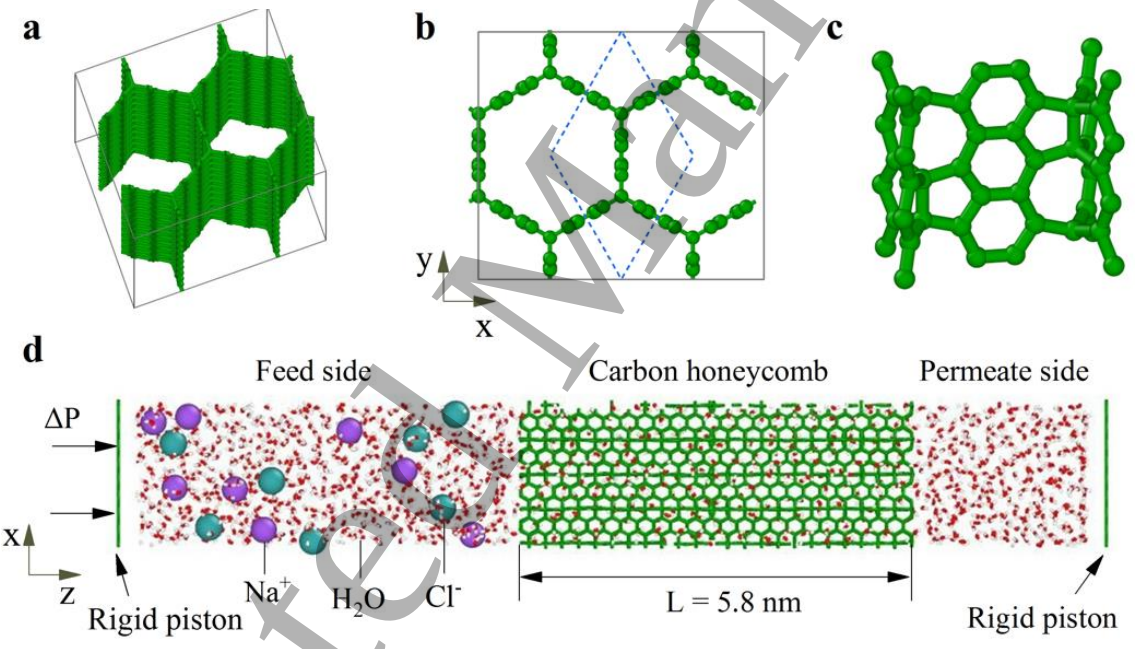

Figure 1. Simulation box and water desalination performance: (a) Angled and (b) vertical view of CHC; (c) Atom structure of the wall and junction of CHC; (d) Schematic of the simulation box consisting of a CHC, water, ions (Na^+ and Cl^-) and two graphene sheets.

NEMD simulations are employed to test the performance of CHC as water desalination membranes using the LAMMPS package [29, 30]. The post-processing including water flux, salt rejection and water molecules distribution is studied with

OVITO [31, 32]. We have used our resources to run three times for every case, and for each case, three MD simulations were performed by changing the initial conditions to achieve meaningful insights.

The interactions between the water molecules are described by the TIP4P model, and the salt ions are described by the non-polarizable model. The AIREBO potential [33] is utilized to describe the interactions between the carbon atoms. For other kinds of atoms, the Lennard Jones (LJ) and Coulombic terms are utilized [34-36]. The interaction energy $U(r_{ij})$ is given as [37]:

$$U(r_{ij}) = 4\varepsilon_{ij}\left[\left(\sigma_{ij}/r_{ij}\right)^{12} - \left(\sigma_{ij}/r_{ij}\right)^{6}\right] + \frac{q_i q_j}{\varepsilon r_{ij}} \quad (1)$$

where ε_{ij} and σ_{ij} are the energy and length parameters, r_{ij} is the distance between the atoms i and j, q_i and q_j are the charges on the two atoms and ε is the dielectric constant. The LJ parameters between the different elements are estimated by using the Lorentz Berthelot mixing rules. The LJ parameters are summarized in Supplementary Table S1. The canonical (NVT) ensemble is used for the simulations with a Nose Hoover thermostat of 50 fs at T=300 K. The periodic boundary conditions are employed in all three directions of the simulated box, with a time step of 0.5 fs. Five different external pressures (ranging from 50 to 250 MPa) are applied on the graphene piston to achieve the water desalination process, and the pressure on the graphene piston on the fresh water side is keept at 0.1 MPa (1 atm). The simulation time is related to the applied pressure. The greater is the pressure, the shorter is the time taken by water to pass. 10,000,000 time steps are taken for each NEMD simulation.

It has been reported that the salt rejection is more important than water permeability for water desalination, which is calculated by [7]:

$$\text{Salt rejection} = (1 - \frac{n_{\text{Perment Ions}} / n_{\text{Ions}}}{n_{\text{Perment Water}} / n_{\text{Water}}}) \times 100\% \quad (2)$$

where $n_{\text{Perment Ions}}$ and $n_{\text{Perment Water}}$ represent the number of ions and water molecules which have passed through CHC when half of the water has flowed to the permeate side, whereas n_{Ions} and n_{Water} represent the number of ions and water molecules in the feed side at the beginning of the simulations.

3. Results and Discussion

3.1 *Effect of pressure*

Applied pressure has a significant influence on the performance of the water desalination performance of the membrane. Varying external pressures were applied to the two rigid graphene pistons in the cell axis direction so that the system is in a non-equilibrium condition with a hydrostatic pressure difference across the CHC. The number of water molecules filtered through the CHC (length L = 5.8 nm) pores as a function of time for different pressure values is presented in Figure 2(a). Each curve in Figure 2(a) starts in the linear state with a near constant water flow rate. This suggests that the impact of the gradually increased salinity in the feed side could be negligible in this region. The water flow rate is estimated by the slope of each curve in Figure 2(a). With time, the water molecules pass through CHC to the permeate side with increasing salinity in the feed side, following the osmotic gradient enhancement. Therefore, the driving force that causes the water molecules to flow is reduced, and the slope of the water molecules number vs. time curves decreases. At an externally applied pressure of 50 MPa, the water density and distribution of the oxygen atoms along the radial direction in a single pore are exhibited in Supplementary Figure S2 and S3, respectively. The results show that the water

molecules are mainly distributed in the range of 1.6 to 2.4 Å from the center of the CHC pore.

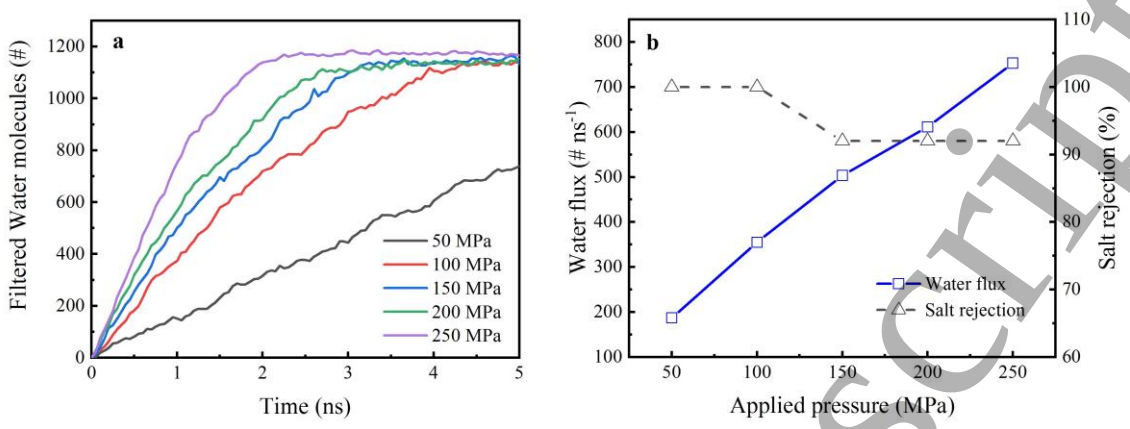

Figure 2. (a) The number of the water molecules filtered through the CHC pores as a function of simulation time at different pressures and (b)Water flux and salt rejection as a function of the applied pressure for CHC.

The water flux is calculated when the half of the water molecules have entered the permeate region, using the slopes from Figure 2(a). The effective water flux values achieved in each simulation are illustrated in Figure 2(b). The results indicate that the water flux is nearly linear with the applied pressure, which is consistent with the previous studies [11].

Moreover, it has been reported that the salt rejection is more important than the water permeability for the desalination membranes [7]. The dashed line in Figure 2(b) shows the salt rejection as a function of the applied pressure. The result shows that at low pressures, CHC has a perfect salt rejection with no salt ions passing before half of the water has flowed through CHC. On increasing the applied pressure up to 150 MPa, the salt rejection reduces only to 92%. This can be explained by considering the free energy profile of an ion and water molecule passing through the CHC membrane. As expected, the higher pressure provides enough energy to the salt ions to pass through the nanoporous

membrane, however, at a very low extent. These results show that CHC could be an effective water desalination membrane alternative.

A few previous MD studies have shown that the water flux through CNT is affected by the length [8, 38]. In this study, the considered CHC lengths are 5.8, 11.6 and 58 nm respectively. The water flux of CHC with varying lengths as a function of applied pressure is shown in Figure 3(a). The decay of the water flux with increasing CHC length shows similar behaviour for different pressure values. As the length increases, the water flux is obviously noted to decrease. For CHC with a length of 58 nm, the water flux is noted to reduce by 17% as compared to CHC with a length of 5.8 nm at a pressure of 50 MPa. The reduction is observed to be higher on increasing the applied pressure. The maximum reduction of water flux is noted to be about 39% at 250 MPa. It has been reported that the use of the Nose-Hoover thermostats may overestimate the reduction in the water flux of the nanoporous carbon materials on increasing the length [8]. Therefore, the effective water permeability of CHC might be larger, if the similar effect occurs with CHCs.

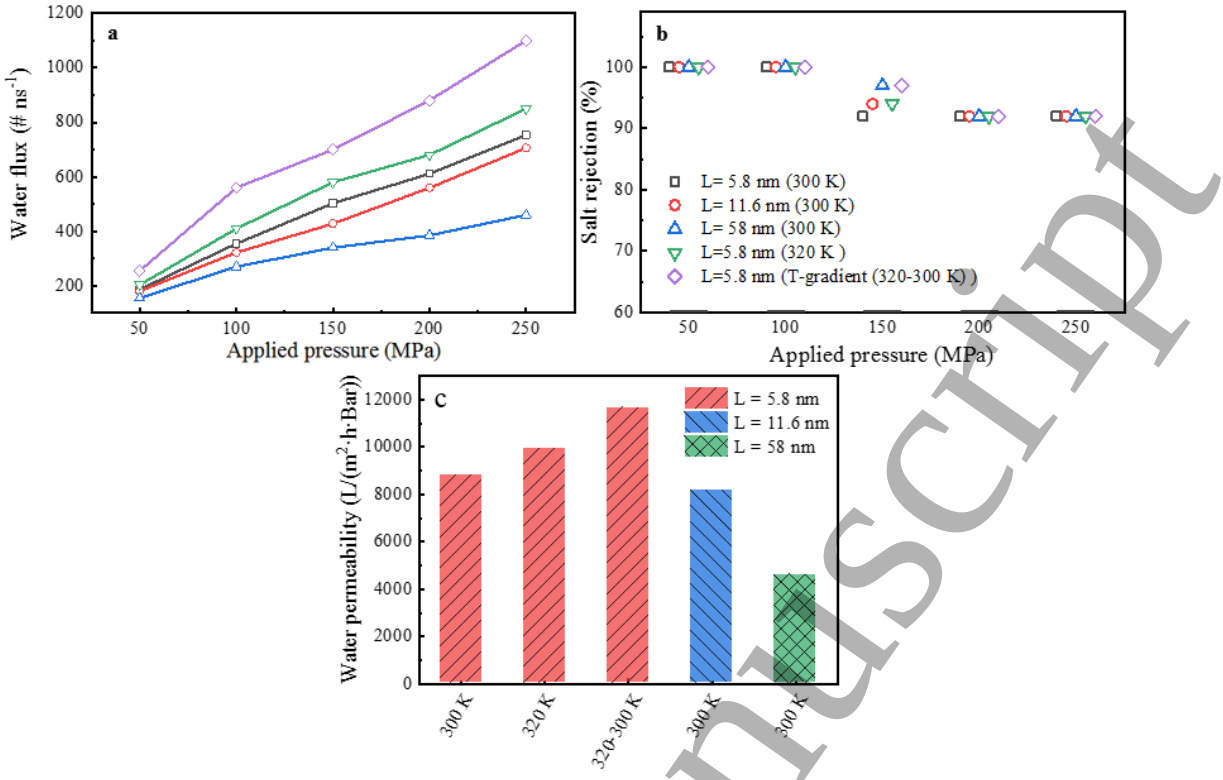

Figure 3. Length and temperature dependence: Water flux (a) and salt rejection (b) as a function of the applied pressure for CHCs with different lengths at different temperature conditions; (c) Water permeability of CHC at different conditions.

At 300 K, the water permeability of CHCs with different lengths is described in Figure 3(c). As the CHC length increases, the water permeability decreases, exhibiting the same trend as reported for CNT for water transportation by Su [38]. Remarkably, the water permeability of CHC with a length of 58 nm is 48% lower than that of 5.8 nm. It shows the water flow through CHC is frictional [39].

The salt rejection as a function of the applied pressure is depicted in Figure 3(b). Meanwhile, the membranes with CHC lengths of 11.6 nm and 58 nm length exhibit a perfect salt rejection, while the salt rejection of the CHC with 5.8 nm length is about 92% at 150 MPa. Similar salt rejection under other applied pressures is observed, indicating that the salt rejection is less affected by the CHC length.

3.2 *Effect of temperature gradient*

Increasing temperature enhances the diffusion process of both water and salt ions. It has been reported [15] that an axial temperature gradient can induce a fast and continuous water flow through CNT. Here, the effect of the temperature gradient on the performance of CHC for water desalination has been investigated. Simulations under the temperatures of 300 K and 320 K are taken as two reference groups. In order to discuss the effect of the temperature gradient, a different thermostat for each region is considered. The atoms in the feed and permeate sides are heated to 320 K and 300 K, respectively. The atoms in the middle region are controlled by the microcanonical (NVE) ensemble. This process is noted to induce the temperature gradient of 3.5 K/nm in the water desalination system.

Water flux values at different temperature conditions are depicted in Figure 3 (a). The results show that the larger water flux values are noted at 320 K than 300 K. The kinetic energy of the water molecules increases with temperature, which makes it easy for the water molecules to pass through. Thus, a higher water flux is noted at higher temperatures. The large pressure gradients can induce flow in CHC, so does the temperature gradient in this study. In order to optimally reflect the effect of temperature gradient on the water flux, we have further considered two temperature gradients (310-300 K and 330-300 K) at 50 MPa. The results show that the water flux increases on increasing the temperature gradient, as shown in Supplementary Figure S4.

In Figure 3(c), the water permeability of CHC has been plotted. The results show that the water permeability of CHC at 320 K is 13% higher than 300 K. The introduction of the temperature gradient improved the water permeability of CHC by 33%, indicating that the temperature gradient can promote the water permeability more effectively than simply raising the temperature.

Previous study [40] has shown that the gases in CNT flow by applying traveling waves. Qiu et al. [41] found that the key to the water flow is the amplitude at the free end of CNT, which is induced by applying periodic force. The higher the amplitude, the greater is the water flux. Elton et al. [15] noted that the water flow in the temperature gradient direction within CNT can be caused by the difference in the amplitude of the oscillation between the high and low temperature zones. As the applied temperature gradient increases, the amplitude of the oscillations also increases, thus, causing the higher water flow rates. Here, the thermal Brownian ratchet concept [42] is also suitable for the use of CHC for water desalination. By the induced temperature gradient, the water permeability also increases obviously. The introduction of the temperature gradient, thus, promotes the flow of water in CHC.

The Soret coefficient is calculated to quantify the effect of the temperature gradient on the water flux of CHC. The Soret coefficient is defined as [16]:

$$S = D_t / D \tag{3}$$

where D_t and D are the thermal and isothermal diffusion coefficients respectively. The isothermal diffusion coefficient D is obtained from the classical mean square displacement:

$$D = \lim_{t\to\infty} \frac{1}{6Nt} \left\langle \sum_{j=1}^{N} \left| r_j(t) - r_j(0) \right|^2 \right\rangle \tag{4}$$

where $r(t)$ is the displacement of the atom j at time t and N is the number of atoms. The coefficient of thermal diffusion is calculated from the equation:

$$D_t = V/\Delta T \tag{5}$$

where V is the water flow rate determined by the water flux during the simulation. The isothermal diffusion coefficient is 2.8 nm^2/ns, which is consistent with the previous reports for water under nanoscale confinement (0.9-8.8 nm^2/ns) [14, 43]. The water flux induced by the temperature gradient under zero driving pressure is about 50 molecules/ns, corresponding to the water flow rate of 1.16 nm/s. Thus, the extracted thermal diffusion coefficient is 0.33 $nm^2/(ns\ K)$, which corresponds to a Soret coefficient of 0.12 K^{-1}. The observed value is one order of magnitude lower than the simulated coefficient for the confined water inside CNT [14], however, it is closer to the value for the binary Lennard-Jones liquids [44] and the experimental results for the water-methanol mixtures [16].

The salt rejection as a function of both temperature and applied pressure is plotted in Figure 3(b). It is found to be 100 % for the applied pressure below 100 MPa. It is owing to the fact that the smaller values of pressure induce smaller forces on the salt ions to pass through CHC. The salt rejection makes a little difference at 150 MPa, where the temperature gradient shows a 100% salt rejection, which is higher than observed for 300 K and 320 K.

3.3 *Porosity and water permeability*

The water permeability is another important factor for the water desalination performance. Figure 4 shows the water permeability for various nanoporous carbon materials (hydroxylated and hydrogenated graphene [10], MoS_2, graphene [11], CNT [7] and graphyne [9]) including CHC with L = 5.8 nm calculated in this study. CHC shows a better water permeability performance than the 2D membranes of graphene, MoS_2, graphene with hydroxylated or hydrogenated pores and graphyne-5, with similar pore area. For 2D nanoporous materials, the pores tend to weaken the material by reducing its structural strength. It was reported that both strength and Young's modulus of the nanoporous graphene reduce on increasing the pore radius [3]. It is important for a

material to be strong in order to maintain its mechanical structure under high hydraulic pressure inherent to the reverse osmosis desalination process. Thus, the porosity of such materials is generally small. This, thus, greatly limits water permeability of these materials. For instance, the water permeability of graphene with a 10% porosity is about 1000 L/(m^2·h·Bar) [10].

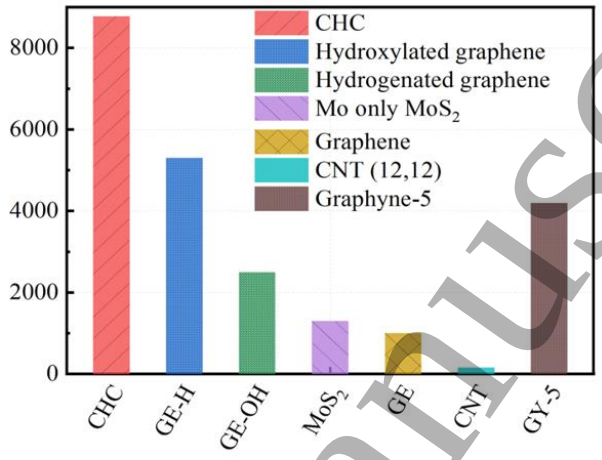

Figure4. The performance of various membranes with similar single area for water desalination at 300 K. The single pore area of CHC is 78 Å2 with L = 5.8 nm. The pore area of the hydroxylated and hydrogenated graphene [10], MoS2 and graphene [11] is 62, 50, 56 and 60 Å2 respectively, and the corresponding permeability is calculated assuming a 10% porosity. The pore area of CNT (12,12) [7] and Graphyne-5 [45] is 62 and 77 Å2.

However, it is generally less critical to focus on the strength of CHC due to its unique nanoporous structure. The stress-strain curves along different directions show that CHC has outstanding structural strength (as shown in Supplementary Figure S5). In this study, CHC has a nanopore density of 1.15×10^{14} cm^{-2}, while it is 1.7×10^{13} cm^{-2} for graphene [3], 7.9×10^{13} cm^{-2} for graphyne-5 [9] and only 2.5×10^{11} cm^{-2} for CNT [7] with similar pore area. For simplicity, the porosity is expressed by the ratio of the hole area and total cross-sectional area, where the hole area is calculated by the area of the inscribed circle of the hole. The calculated porosity of CHC is noted to be about 64%, whereas it is 43% for graphyne-5, 10% for graphene and only 0.5% for CNT.

Benefitting from the specific structure, the CHC membrane has a relatively high porosity, while maintaining a high stiffness. Therefore, CHC is noted to have a higher

water permeability as compared to other materials. It has been reported that with a thickness of 3 nm and a diameter of 1.6 nm, CNT has a water permeability about 160 L/(m^2·h·bar) [7], which is more than one order of magnitude lower than CHC with similar pore area.

4. Conclusions

A promising performance of CHC for water desalination has been predicted by means of molecular dynamics simulations. Benefitting from the specific structure of an array of honeycomb holes, the CHC membrane is noted to possess a relatively high porosity with high stiffness. To the authors' best knowledge, the water permeability of CHC is greater than other carbon materials and reverse osmosis membranes. The water transport through CHC is pressure dependent. Besides, the water permeability of CHC increased by inducing the temperature gradient, thus, providing a promising approach to improve the water flux. CHC shows high salt rejection for the applied pressure of less than 150 MPa. Overall, the newly developed CHC based water desalination membrane exhibits strong potential for seawater desalination and water transportation, along with application to the nanofluidic devices.

Acknowledgments

This work was supported by the National Key R&D Program of China (Grant No. 2020YFA0405700). Q. P. would like to acknowledge the support provided by the Deanship of Scientific Research (DSR) at King Fahd University of Petroleum & Minerals (KFUPM) through project No. DF201020.

The conflict of interest statement

The authors declare that they have no known competing financial interests or personal relationships that could have appeared to influence the work reported in this paper.

References

[1] J.R. Werber, A. Deshmukh, M. Elimelech, The Critical Need for Increased Selectivity, Not Increased Water Permeability, for Desalination Membranes, Environmental Science & Technology Letters 3(4) (2016) 112-120.

[2] J.R. Werber, C.O. Osuji, M. Elimelech, Materials for next-generation desalination and water purification membranes, Nature Reviews Materials 1(5) (2016).

[3] Cohen-Tanugi D 2015 Nanoporous graphene as a water desalination membrane *PhD* Massachusetts Institute of Technology, Cambridge

[4] L. Malaeb, G.M. Ayoub, Reverse osmosis technology for water treatment: State of the art review, Desalination 267(1) (2011) 1-8.

[5] K.P. Lee, T.C. Arnot, D. Mattia, A review of reverse osmosis membrane materials for desalination—Development to date and future potential, Journal of Membrane Science 370(1) (2011) 1-22.

[6] K. Gethard, O. Sae-Khow, S. Mitra, Water desalination using carbon-nanotube-enhanced membrane distillation, ACS Appl Mater Interfaces 3(2) (2011) 110-4.

[7] M. Thomas, B. Corry, A computational assessment of the permeability and salt rejection of carbon nanotube membranes and their application to water desalination, Philos Trans A Math Phys Eng Sci 374(2060) (2016).

[8] M. Thomas, B. Corry, Thermostat choice significantly influences water flow rates in molecular dynamics studies of carbon nanotubes, Microfluidics and Nanofluidics 18(1) (2014) 41-47.

[9] J. Kou, X. Zhou, Y. Chen, H. Lu, F. Wu, J. Fan, Water permeation through single-layer graphyne membrane, J Chem Phys 139(6) (2013) 064705.

[10] D. Cohen-Tanugi, J.C. Grossman, Water desalination across nanoporous graphene, Nano Lett 12(7) (2012) 3602-8.

[11] M. Heiranian, A.B. Farimani, N.R. Aluru, Water desalination with a single-layer MoS2 nanopore, Nat Commun 6 (2015) 8616.

[12] Q. Shi, H. Gao, Y. Zhang, Z. Meng, D. Rao, J. Su, Y. Liu, Y. Wang, R. Lu, Bilayer graphene with ripples for reverse osmosis desalination, Carbon 136 (2018) 21-27.

[13] Y. Wang, Z. He, K.M. Gupta, Q. Shi, R. Lu, Molecular dynamics study on water desalination through functionalized nanoporous graphene, Carbon 116 (2017) 120-127.

[14] H.A. Zambrano, J.H. Walther, P. Koumoutsakos, I.F. Sbalzarini, Thermophoretic Motion of Water Nanodroplets Confined inside Carbon Nanotubes, Nano Letters 9(1) (2009) 66-71.

[15] E. Oyarzua, J.H. Walther, C.M. Megaridis, P. Koumoutsakos, H.A. Zambrano, Carbon Nanotubes as Thermally Induced Water Pumps, ACS Nano 11(10) (2017) 9997-10002.

[16] J.F. Dutrieux, J.K. Platten, G. Chavepeyer, M.M.J.J.p.c.b. Bou-Ali, On the Measurement of Positive Soret Coefficients, J Phys Chem B 106(23) (2002) 6104-6114.

[17] S. Duhr, D. Braun, Why Molecules Move along a Temperature Gradient, Proceedings of the National Academy of Sciences of the United States of America 103(52) (2006) 19678-19682.

[18] N. Park, J. Ihm, Electronic structure and mechanical stability of the graphitic honeycomb lattice, Physical Review B 62(11) (2000) 7614-7618.

[19] J. Hu, W. Wu, C. Zhong, N. Liu, C. Ouyang, H.Y. Yang, S.A. Yang, Three-dimensional honeycomb carbon: Junction line distortion and novel emergent fermions, Carbon 141 (2019) 417-426.

[20] N.V. Krainyukova, E.N. Zubarev, Carbon Honeycomb High Capacity Storage for Gaseous and Liquid Species, Phys Rev Lett 116(5) (2016) 055501.

[21] L. Xie, H. An, C. He, Q. Qin, Q. Peng, Mechanical Properties of Vacancy Tuned Carbon Honeycomb, Nanomaterials 9(2) (2019).

[22] X.K. Chen, J. Liu, D. Du, Z.X. Xie, K.Q. Chen, Anisotropic thermal conductivity in carbon honeycomb, J Phys Condens Matter 30(15) (2018) 155702.

[23] S. Wang, D. Wu, B. Yang, E. Ruckenstein, H. Chen, Semimetallic carbon honeycombs: new three-dimensional graphene allotropes with Dirac cones, Nanoscale 10(6) (2018) 2748-2754.

[24] Z. Pang, X. Gu, Y. Wei, R. Yang, M.S. Dresselhaus, Bottom-up Design of Three-Dimensional Carbon-Honeycomb with Superb Specific Strength and High Thermal Conductivity, Nano Lett 17(1) (2017) 179-185.

[25] Z. Zhang, A. Kutana, Y. Yang, N.V. Krainyukova, E.S. Penev, B.I. Yakobson, Nanomechanics of carbon honeycomb cellular structures, Carbon 113 (2017) 26-32.

[26] Q. Qin, A. Haojie, H. Chenwei, X. Lu, P. Qing, Anisotropic and temperature dependent mechanical properties of carbon honeycomb, Nanotechnology 30(32) (2019).

[27] H. Wang, Q. Cao, Q. Peng, S. Liu, Atomistic Study of Mechanical Behaviors of Carbon Honeycombs, Nanomaterials 9(1) (2019).

[28] R. S. Weatherup, 2D Material Membranes for Operando Atmospheric Pressure Photoelectron Spectroscopy, Topics in Catalysis 61(20) (2018) 2085-2102.

[29] S. Plimpton, Fast Parallel Algorithms for Short-Range Molecular Dynamics, Journal of Computational Physics 117(1) (1995) 1-19.

[30] Q. Peng, F. Meng, Y. Yang, C. Lu, H. Deng, L. Wang, S. De, F. Gao, Shockwave generates < 100 > dislocation loops in bcc iron, Nat Commun 9(1) (2018) 4880.

[31] A. Stukowski, Visualization and analysis of atomistic simulation data with OVITO–the Open Visualization Tool, Modelling and Simulation in Materials Science and Engineering 18(1) (2010) 015012.

[32] L. Xie, H. An, Q. Peng, Q. Qin, Y. Zhang, Sensitive five-fold local symmetry to kinetic energy of depositing atoms in Cu-Zr thin film growth, Materials 11(12) (2018) 2548.

[33] W.B. Donald, A.S. Olga, A.H. Judith, J.S. Steven, N. Boris, B.S. Susan, A second-generation reactive empirical bond order (REBO) potential energy expression for hydrocarbons, Journal of Physics: Condensed Matter 14(4) (2002) 783.

[34] T.A. Beu, Molecular dynamics simulations of ion transport through carbon nanotubes. I. Influence of geometry, ion specificity, and many-body interactions, J Chem Phys 132(16) (2010) 164513.

[35] W.L. Jorgensen, J. Chandrasekhar, J.D. Madura, R.W. Impey, M.L. Klein, Comparison of simple potential functions for simulating liquid water, The Journal of Chemical Physics 79(2) (1983) 926-935.

[36] J. In Suk, T.E. Cheatham, Determination of alkali and halide monovalent ion parameters for use in explicitly solvated biomolecular simulations, J Phys Chem B 112(30) (2008) 9020.

[37] D. Frenkel, B. Smit, Understanding molecular simulation: from algorithms to applications. 2nd ed. Physics Today 50(7) (1996).

[38] J. Su, H. Guo, Effect of nanochannel dimension on the transport of water molecules, J Phys Chem B 116(20) (2012) 5925-32.

[39] R. Wan, H. Lu, J. Li, J. Bao, J. Hu, H. Fang, Concerted orientation induced unidirectional water transport through nanochannels, Phys Chem Chem Phys 11(42) (2009) 9898-902.

[40] Z. Insepov, D. Wolf, A. Hassanein, Nanopumping Using Carbon Nanotubes, Nano Letters 6(9) (2006) 1893-1895.

[41] H. Qiu, R. Shen, W.J.N.R. Guo, Vibrating carbon nanotubes as water pumps, Nano Research 4(3) (2011) 284-289.

[42] C. S. Peskin, G. M. Odell, G. F. Oster, Cellular Motions and Thermal Fluctuations: The Brownian Ratchet, Biophys Journal 65 (1993) 316–324.

[43] A. Striolo, The Mechanism of Water Diffusion in Narrow Carbon Nanotubes, Nano Letters 6(4) (2006) 633-639.

[44] D. Reith, F. Müller-Plathe, On the nature of thermal diffusion in binary Lennard-Jones liquids, The Journal of Chemical Physics 112(5) (2000) 2436-2443.

[45] J. Kou, X. Zhou, H. Lu, F. Wu, J. Fan, Graphyne as the membrane for water desalination, Nanoscale 6(3) (2014) 1865-70.